J. Basic. Appl. Sci. Res., 4(7)218-230, 2014
© 2014, TextRoad Publication
ISSN 2090-4304
Journal of Basic and Applied Scientific Research
www.textroad.com

Numerical Simulation of Convective Natural Ventilation in a Light Well Connected to a Horizontal Void: Comparison of Various RANS-Based Turbulence Models

Tareq Farea[a*], Dilshan Ossen[a], Saqaff Alkaff[b], Fatemeh Ghadikolaei[a,c], Yakubu Dodo[a]

[a]Department of Architecture, Faculty of Built Environment, Universiti Teknologi Malaysia, Malaysia
[b]Department of Mechanical, Faculty of Engineering & Technology, Multimedia University, Malaysia
[c]Department of Architecture, Faculty of engineering, Islamic Azad University- Sari Branch, Sari, Iran

Received: May 18, 2014
Accepted: June 21, 2014

ABSTRACT

Lightwell or deep courtyard is commonly used in high-rise buildings and usually implemented to admit daylight and to derive natural ventilation. Since attention is being given to energy saving, use of natural ventilation has become one of the most fundamental strategies. This paper aims to evaluate various numerical turbulence models used to predict natural ventilation in a lightwell connected to the outdoor through a bottom horizontal void as inlet gap and a top skylight outlet. A 3-D steady state modeling was carried out using Computational Fluid Dynamics (CFD) to simulate the airflow inside the lightwell. Six different Reynolds-Averaged Navier–Stokes (RANS) turbulence models were validated with experimental data from literature in order to identify the most appropriate turbulence model for this type of airflow. Results showed that all RANS models have the capability to simulate convective natural ventilation in the lightwell. However, Re-normalized Group (RNG) *k-ε* model gave the best overall simulation performance in terms of the ability to capture the airflow pattern, predict the air temperature and airflow rate inside the lightwell. The results also demonstrate that CFD modeling utilizing the RANS-based models, when appropriately selected for the most suitable model, is a reliable tool for predicting airflow pattern, airflow rate and temperature inside the lightwell.

KEY WORDS: CFD, validation, high-rise building, lightwell, horizontal void, turbulence models.

Symbols list

Q	flow rate (m^3/h)	κ	von Karman constant (= 0.4187)
T	temperature (^oC)	θ	temperature fluctuation (^oC)
k	turbulent kinetic energy (m^2/s^2)	ε	dissipation of k (m^2/s^3)
g	acceleration due to gravity (m/s^2)	β	coefficient of thermal expansion (K^{-1})
Pr	Prandtl number	μ	dynamic viscosity (Pa.s)
Re	Reynolds number	ν	kinematic viscosity (m^2/s)
u	mean air velocity magnitude (m/s)	γ	intermittency
u'	velocity fluctuation component (m/s)	α^*	turbulent viscosity damping factor
t	temperature fluctuation component (^oC)	ρ	mass density (kg/m^3)
S_{ij}	strain rate tensor (1/s)	ω	specific dissipation rate (s^{-1})
$\overline{(\,)}$	time average	σ	turbulent Pr for k or ω
Γ	diffusion coefficient	δ	Kronecker delta
Ω	magnitude of rotation tensor		

1. INTRODUCTION

Natural ventilation is one of the most fundamental strategies in building [1, 2] which contributes to reduction of the energy consumption required for mechanical equipment such as fans and air-conditioners. Recently, passive design strategies received more attention in the first stage of building design in order to optimize its performance in terms of inducing natural ventilation inside and around the buildings. Lightwell is a vertical shaft commonly used in high-rise residential buildings [3], especially in deeper-plan buildings, to admit daylight and to induce natural ventilation. The lightwell space connects directly to the outdoor from the top. However in most buildings the lightwell is underutilized as a possible means of improving the air flow within the buildings. It has been noted that proper configuration of lightwell and the

***Corresponding Author:** Tareq Farea, Department of Architecture, Faculty of Built Environment, Universiti Teknologi Malaysia, Malaysia. E-mail *tareqgfarea@*outlook.com

outlet will not only improve the airflow inside the lightwell itself[4], adjoining rooms[5]and thus cool down the building structure [6] but will also change the wind environment around the high-rise building [7]. In addition, studies showed that the courtyard, lightwell and atrium as buffer zones provide natural ventilation for adjoining spaces (e.g. [4, 8-13]).

Natural ventilation can be generated in and around buildings by two strategies; wind force and thermal buoyancy or by the combination of them, which are called natural convection[14, 15].Liu, Ford [16]studied natural ventilation in three floor-high atrium based on only buoyancy-induced airflow and they concluded that this strategy alone is not enough to support natural ventilation, particularly in hot and humid climate due to small temperature difference. The study suggested that the ventilation would be more effective in higher atrium as higher temperature differences, especially when it is supported by wind-induced strategy. According to Etheridge [17], most of the previous studies on natural ventilation in last years have gave more focus on buoyancy-induced airflow which usually is not enough to improve internal natural ventilation especially in those regions with low air temperature differences. There is therefore the need to study both natural ventilation strategies (wind and buoyancy forces induced). This is especially in regions with low wind velocity and low temperature differences such as the tropical countries in Southeast Asia[15, 18].

Chen (2009) identified seven different methods for predicting airflow characteristics in the built environment. These methods are based on theoretical analysis (e.g.[19, 20]), experimental measurement (e.g.[21-23]) and computational simulation (e.g. [12, 24-28]). Although small-scale and full-scale experimental models are the most reliable methods, CFD has been the most commonly used method in the last decade [29]. Selecting the appropriate CFD approach and a turbulence model are the most critical factors in fluid flow studies [30, 31]. Therefore, before a CFD model is used to examine a flow situation, it is necessary that the model be validated by experimental or theoretical models to ascertain the integrity [29, 32-34]. Previous studies have recommended validation of CFD model results with measured data obtained by experimental approaches [17, 29, 33]. Experimental validation by full-scale models requires more man-efforts and high cost in addition to the difficulty of controlling the boundary conditions of outdoor environment [17, 35-37]. As a result, many studies opt to use small-scale experimental measurement in order to validate results from CFD simulation (e.g. [34, 37-40]). However, small-scale model test using the wind tunnel presents some difficulty in the ability to simulate the real wind profile and turbulence level as well as heat generation inside and around the model. Some small-scale experimental studies were based only on wind force, with the thermal aspect neglected [17]as its difficult to effect heat generation in the wind tunnel and control it in a specific zone within the model [41]. Many previous small-scale experimental studies are available as benchmark experiments [42]. These experiments have been done to test different models and there dimensional characteristics. The experimental data obtained from some of the studies have also been used to validate CFD codes(e.g. [43, 44]).Although turbulence is still one of the unsolved problems of fluid mechanics [45], CFD enables appropriate technique to model and solve turbulent natural convection for many flow configurations.

Many studies evaluated with RANS models have used different shapes and types of enclosures (e.g. [12, 14, 26, 37]). Most of the studies have been conducted in small enclosures such as room, with a few in large enclosures such as atriums and lightwells. The flow in these larger spaces is quite complicated and it has not been adequately studied [46]. In the study of these large enclosures, however, particular attention has not been focused on the most appropriate turbulence model for predicting natural convection in the lightwell connected to the outdoor through a horizontal void. Therefore, the current study compares the performance of various turbulence models in predicting the natural convection flow characteristics in a lightwell connected to the outdoor through a bottom horizontal void.

2. METHODOLOGY

2.1 Experimental settings

The main features and processes involved in the wind tunnel experiment performed by Kotani et al. [47]are presented in this section. Using a small-scale model of a high-rise building with lightwell connected with bottom void, Kotani et al. [47] performed wind tunnel experiment to predict the air temperature and airflow rate as well as airflow pattern in the lightwell. They have used two parameters in the study; air velocity and heat generation. The main objective of their work was to estimate the validity of modifying simple calculation for predicting the airflow and air temperature in the lightwell. The high-rise building is about a forty-storey building with square plan and has dimensions 36 x 36 x 120 m^3 (width x depth x height). The lightwell in the core of the building passes vertically through all the floors without any openings except the bottom lateral horizontal void (one side open in windward direction) and the top vertical outlet. The building model for the wind tunnel experiment was scaled to 1:250. The outline of the model therefore has dimensions 144 x 144 x 480 mm^3. The volume of the lightwell and the area of the horizontal void are dimensioned 72 x 72 x 468 mm^3 and 72 x 12 mm^2 (width x height) respectively (Fig. 1).

The wind profile was experimentally generated and it was expressed by power law of one-fourth. Large-scale turbulence was generated by lattice and roughness elements in the wind tunnel floor, which corresponded to wind above towns. For this purpose, a long wind tunnel, about 7.756 m in length, which has a test section of dimensions 1.4 x 1.6 (H) m^2 was used. The experimental conditions were specified in terms of rate of heat generation in the lightwell ranging from 10 – 40 W, and wind velocity in the wind tunnel which ranged from 0 – 1.5 m/s. The wind direction in all cases was perpendicular to the windward façade where the horizontal void was located. They used laser light sheet and tobacco smoke to visualize the airflow pattern and photo acoustic infrared detection method to measure the airflow rate in the lightwell. To measure air temperature, five thermocouples were set vertically in the lightwell. For more detailed information about the experimental settings, refer to Kotani et al. [47]. Some of the experimental results will be presented together with numerical results later for comparison.

2.2 Numerical simulation

A commercial CFD code ANSYS® Fluent14.0 was used to perform the simulation of airflow and temperature in the lightwell. Steady-state airflow and heat transfer through a three-dimensional model was carried out. No-slip boundary condition was set on the walls. Heat generation and reference air velocity used in the numerical study were 40 W and 1.5 m/s, respectively, as highest values of the experimental study range.

The numerical study contains two main steps; sensitivity analysis and turbulence models comparisons and examining the effect of mesh size on the results of each turbulence model. In sensitivity analysis different parameters were examined. The RNG k-ε was initially used in all simulation sensitivity analyses as most commonly used in literature. After the RNGk-ε simulation has yielded results comparable with experimental data then the other five turbulence models were examined and their results also compared with the experimental data.

2.2.1 Flow domain and geometry

Similar dimensions of the building model and the wind tunnel as used in the experimental study have been used in the CFD validation, except the windward and leeward distances (i.e. the distance between the domain inlet and the windward building surface). Therefore, the test section dimensions of the wind tunnel (1.4x1.6h m^2) have been fixed as shown in Fig. 1. Thus, the windward and leeward distances in the computational domain were set as recommended in the literature. Based on previous studies(e.g. [13, 26, 48]) the windward and the leeward distances of the model were 5h and 10h respectively, where h is the height of the building. Franke, Hellsten [48]have also recommended 15h for the leeward distance in order to ensure the flow has become fully redeveloped behind the building. However, 10$h$as a maximum distance was set behind the building because of the large domain size and thus the extra computational time required for modeling a high-rise building. In addition, recommended dimensions in all directions were also examined by changing the cross section of the flow domain. Nevertheless, a trial and error verification process has been recommended [49]. For this purpose, four different sizes of domain were examined and the results compared with experimental data. Three of these domains were examined with fixed cross section of the wind tunnel and one is the largest as recommended. Fig. 1 shows the three sizes with fixed cross section and distances of the velocity inflow and the outflow from the building surfaces in the windward and leeward, respectively. The distances of these three sizes were set in the windward and leeward directions, respectively as followed: a) the small-sized domain, 1 h and 2 h; b) the medium-sized domain, 2 h and 4 h; and c) large-sized domain, 5 h and 10 h. In the large recommended domain the boundary was set 5 h from both sides and roof surfaces of the building to the domain boundaries and windward and leeward distances were also set at 5 h and 10 h, respectively.

Airflow rate and temperature results in the lightwell for each of the four domain sizes were compared with experimental data. Fig. 2 shows that the medium-sized domain produced results that are most close to experimental data. Although, the largest domain (with different cross section) obtained temperature most close to experimental data it has large discrepancy of airflow rate if compared with the other sizes. It should be noted here that each of the domain size was discretized with the same mesh size and growth rate of the cells, resulting in different number of meshes which depend on the size of the domain as shown in Fig. 1. Therefore, the medium-sized domain was selected to compare the six turbulence models in order to save computation time while at the same time producing good results.

2.2.2 Grid discretization

The computational domain was discretized using an unstructured grid with high resolution in the lightwell and the horizontal void, where high-gradient flow zone exists. A growth rate of 1.1% in all directions from these zones was implemented for the meshes. The spatial domain was divided into tetrahedral elements. Nevertheless, grid sensitivity test was carried out with different numbers of cells. Fig.

3 shows some of the different types of meshes used, ranging from coarser to finer grids, with the enlarged view of the meshes at the bottom of the lightwell and the horizontal void. The mesh types are made up of $18x10^4$ (180k), $45x10^4$ (450k), $63x10^4$ (630k) and $1.2x10^6$ (1.2 mil) cells. The results for calculations employing these mesh types were compared with experimental data. Fig. 4 shows that the grid with 450k meshes is the most appropriate one as its results of air temperature and airflow rates in the lightwell were the closest to experimental data. The upwind scheme of second-order accuracy and SIMPLE solution algorithm were used for the convection terms while the least square cell-based gradient for spatial discretization was used for the diffusion terms of the governing equations.

2.2.3 Boundary conditions

To generate a wind profile that corresponds to experimental data, User Definition Function (UDF) available in Fluent was used to set the one-fourth power law for a reference velocity of 1.5m/s. Turbulence was specified using "Intensity and Hydraulic Diameter" for all the turbulence models. The value of the turbulence intensity was fixed at 10% as an approximation to experimental data, while the hydraulic diameter was calculated as 1. However, simulation was examined with a turbulence intensity of 15% but there was no significant difference in the set of results obtained from calculations employing the lower value. In addition to these solver settings the intermittency was fixed at 1 for the SST model as the study considered a fully turbulent flow, while for the RSM "*k* or Turbulence Intensity" was specified as the Reynolds-Stress Specification Method.

In the experimental study, heat was generated by two coiled wire fixed symmetrically along the vertical axis in the lightwell. Numerically, it is difficult to simulate the heat released from the coiled wire. Therefore, two different methods provided in Fluent have been used to effect heat generation in the lightwell that corresponds to those provided in the experiment. These are by prescribing surface heat flux at the inside surfaces of the lightwell, and by specifying volumetric rate of heat generation of the lightwell volume. The results obtained by the two methods were compared with the experimental data and it was found that using heat generation through the lightwell volume is more appropriate for testing the six turbulence models. The prescribed ambient air temperature of 12^oC for the simulation corresponds with that used for the wind tunnel experiment.

2.2.4 Turbulence modeling:

Since the flow in the experiment is turbulent ($R_e > 4000$), the RANS-based models were employed to model of the mean airflow in the lightwell. By RANS approach, for a 3-D steady-state flow, the time-average continuity (mass conservation), Navier-Stokes (momentum conservation) and energy (energy conservation) equations can be written, respectively, as:

$$\frac{\partial}{\partial x_i}\left(\rho u_i\right) = 0 \ , \tag{1}$$

$$\frac{\partial}{\partial x_j}\left(\rho u_j u_i\right) = -\frac{\partial p}{\partial x_i} + \frac{\partial}{\partial x_j}\left(\mu \frac{\partial u_i}{\partial x_j}\right) + \frac{\partial \tau_{ij}^t}{\partial x_j} + \rho g_i \, , \tag{2}$$

$$\frac{\partial}{\partial x_j}\left(\rho u_j T\right) = \frac{\partial}{\partial x_j}\left(\frac{k}{c_p}\frac{\partial T}{\partial x_j}\right) + \frac{\partial q_j^t}{\partial x_j} + S_t \tag{3}$$

where $\tau_{ij}^t = -\rho\overline{u_i' u_j'}$ is turbulent stress tensor, $q_j^t = -\rho\overline{u_j' t}$ is turbulent heat flux, and S_t is the source term for energy .The turbulent stress tensor produced seven additional unknown variables, which means the system of mean flow equations (1-3) are not closed [50]. To be able to solve all the unknowns, additional equations must be introduced into the system of governing equations. Closing the system of equations, on the other hand, leads to the introduction of a number of unknown correlations which must be approximated (modeled) for in terms of the mean flow.

The RANS equations adopt two broad approaches in addressing the closure problem. These are a) direct modeling of each of the turbulent stresses as used in Reynolds Stress Model (RSM), and b) eddy viscosity model, which is based on the Boussinesq hypothesis [50-54], used in developing the other RANS-based models. The RSM has better applications in predicting flow conditions in 3D flows involving large streamline curvature and swirl compared to eddy viscosity models, but it is also more

computationally expensive. The eddy viscosity models are capable of predicting conditions in a range of turbulent shear flows including mixing layers, channel flows, and boundary layers which are the case for the current study. The system of RANS equations and the modeled equations are not easily amenable to analytical solution without over-simplifications which leads to large errors in results. They are therefore most commonly solved by the CFD procedure, adopting an appropriate turbulence model.

The current study employed six of the RANS-based turbulence models to examine their performance for predicting temperature, airflow rate, and airflow pattern in the lightwell connected to a bottom void. These are the one-equation Spallart-Almaras (SA) model, the two-equation Standard *k-ε* (STD *k-ε*), RNG *k-ε*, and SST *k-ω*, the four-equation SST, and the seven-equation RSM (Linear Pressure-Strain). These models have been selected as they are the commonly used in literature. The general form of all the turbulence models used in this study can be written as

$$\rho \frac{\partial \bar{\phi}}{\partial t} + \rho \bar{u}_j \frac{\partial \bar{\phi}}{\partial x_j} - \frac{\partial}{\partial x_j}\left[\Gamma_\phi \frac{\partial \bar{\phi}}{\partial x_j} \right] = S_\phi \qquad (4)$$

where ϕ is the general variable, Γ_ϕ the effective coefficient and S_ϕ the source term of the equation. The mathematical equations for each of the turbulence models are as shown in the appendix. In the appendix only the definitions of the main parameters in each of the model equations have been given. In the RNG *k-ε* model $\mu_{eff} = \mu_t$, for high *Re* flow without swirl, and α_k and α_ε are the inverse effective *Pr* for *k* and ε, respectively. In SST *k-ω* equation, $\alpha^* = 1$ and $\beta^*_\infty = \beta^* = 0.09$ for high *Re* incompressible flow. σ_k and σ_ω are the turbulent *Pr* for *k* and ω, respectively. $Re_{\theta c}$ and F_{length} in the SST equation are functions of transition momentum thickness Reynolds number, $R\tilde{e}_{\theta t}$, where $R\tilde{e}_{\theta t}$ is itself a function of local turbulence intensity.

2.2.5 Near-wall treatments

In order to sufficiently resolve the profiles of turbulent boundary layers near solid region, the near-wall treatment which employs special treatment for the meshes near this region [52]was employed. The use of wall functions is adequate in most cases in describing profiles near solid boundaries [54]. Standard wall functions use dimensionless parameter y+ as wall distance vector. In smooth walls the first grid cell should be within the validity 30 < y+ < 300 (ANSYS® 2011) or 30<y+<500 [53].

2.2.6 Convergence criteria

Convergence was achieved when a sufficient error tolerance initially prescribed following was reached. Previous studies [48, 49] recommended that convergence of the scaled residuals down to 10^{-5} is acceptable. However, for validation studies the use of much lower residuals to reach the converged solution has been recommended [48]. In the current study two convergence criteria with residuals 10^{-5} and 10^{-8} respectively were used and the results compared. It was found that there is no significant differences in the results of air temperature and airflow rate when both convergence criteria were used. In order to reduce the computational time the residual of 10^{-5} has been used to examine the turbulence models.

3. RESULTS AND DISCUSSION

3.1 Airflow pattern

In the experimental model, the acceleration of the flow through the horizontal void followed by the sudden expansion of the air as it exits into the lightwell causes the flow to enter the well with high inertia. This results in flow separation at point A (Fig. 6). The flow is then reflected by the wall and reattaches again to the wall at point B. Due to the separation, a zone of recirculation flow is formed between the main flow and the wall as shown in the experimental model (Fig. 6). In this zone, there occurs acceleration of the main flow inside the well, as a result of the reduction in the flow area. The acceleration increases as well as the heat transfer rate due to the shear layer created between the recirculation zone and the main flow. However, there is increased pressure loss inside the lightwell because of the high curvature and turbulence of the flow in this region.

Fig. 6 compares the results of the various RANS models used in this study with the experimental results of Kotani et al. [47]. As shown from this figure all RANS models were able to capture the airflow pattern comparably well with the experimental study except SST *k-ω* and RSM, especially at the bottom of the lightwell where they failed to predict recirculation as obtained from the experiment. The STD *k-ε* and RNG *k-ε* model have the best agreement with the experimental results in terms of flow pattern. It would be noted

that the shape and size of the recirculation zone are equivalent for both the *k-ε* models and the experiment. However, SA and SST were able to produce the same shape of the recirculation zone but not the size as in the experiment. Although RSM model generated totally different recirculation flows at the bottom, it indicated the ability to capture small recirculation above the building. Nevertheless, none of the models was able to predict the reverse flow in the outlet at the top of the lightwell as observed in the experiment.

3.2 Air temperature results

The diagrams in Fig. 6 show that the RANS models were also able to predict the vertical air temperature distribution in the lightwell, especially at the middle zone along the vertical height of the lightwell, except the SST *k-ω* model which had larger discrepancy at this zone. However, most of the discrepancies observed for all models were at the bottom and top of the lightwell, in the regions of flow separation and reattachment. This has also been reported in many previous studies which found that RANS models are unable to accurately predict flows in these regions.

The RSM model produced results that are in best agreement with experimental results at almost all measured points, followed by the RNG *k-ε* and SST models. Although the RNG *k-ε* model was able to predict temperatures in the lower three-quarters of the height of the lightwell, it could not well capture the temperature values at the top where there exists small reverse flow. The other models: the STD *k-ε*, SA and SST *k-ω*, in this order, followed the SST in their performance ability to predict the air temperature.

3.3 Airflow rate results

Figure 6 also shows the predicted results of the airflow rates in the lightwell using the different RANS-based turbulence models. The results ranged from 2.70 m^3/h for STD *k-ε* to 3.34 m^3/h for SA, while the measured result was 3.28 m^3/h. This gives a maximum discrepancy of about 17.7% with the experimental data as appeared in the STD *k-ε*. However, the SST *k-ω* model shows a discrepancy that is less than 1%, while the SST and SA models gave a discrepancy that is below 2%. The discrepancy indicated for the RNG *k-ε* model is less than 4%. According to previous studies, the range of discrepancy in all the RANS models examined in this study was within acceptable limits except STD *k-ε*.

Some of the turbulence models tend to overestimate the airflow rate, such as the SST, SST *k-ω*, and SA, while the STD *k-ε*, RSM and RNG *k-ε* models tend to underestimate the airflow measured in the lightwell. The calculation model used by Kotani et al. [47] also overestimated the airflow rate, and this they explained was due to some errors which occurred as a result of heat generation in the experiment. They found that the calculated results overestimated measurement by about 38% in the case when the reference air velocity was 1.5 m/s and heat generation was about 40 W. Nevertheless, CFD simulations by the RANS models, under the same conditions, produced discrepancies with the experimental data that were not as high as those of calculations due to Kotani et al. [47].

4. Conclusion:

Systematic validation of some RANS-based turbulence models has been performed using CFD. The numerical results show that the six RANS models have the ability to predict convective natural ventilation in the lightwell space. The models are relatively successful in capturing the separation and reattached flow close to the horizontal void in the lightwell.

The accuracy of air temperature calculated in the region of fluctuating flow significantly depends on the turbulence model selected with the appropriate number of mesh. The RNG *k-ε* model has good capability, in terms of overall simulation performance, in capturing airflow pattern, and predicting airflow rate and temperature distribution in the lightwell compared to other RANS models and this result agree with many previous studies. Nevertheless, the RSM also followed RNG *k-ε* in terms of airflow rate and temperature prediction. Overall, CFD model is a valuable tool for qualitatively and quantitatively predicting natural convection flow in a lightwell connected to a bottom horizontal void. However, further study is recommended to investigate the effect of other configurations on airflow characteristics inside the lightwell such as different horizontal void positions and lightwell segmentation and its size. Since the validity of the results of this study has been based on the agreement of the results with small-scale measurements, full-scale measurements are also needed to capture the actual effects of flow through the lightwell in high-rise buildings.

Acknowledgment:

The authors would like to acknowledge the assistance from Dr. Hisashi Kotani for providing all wind-tunnel experimental data and Dr. Yehia Eldrainy and Mr. Samuel Ayo in Faculty of Mechanical Engineering, Universiti Teknologi Malaysia for the help extended for setting important simulation parameters.

REFERENCES

1. Zhai, Z., 2006. Application of computational fluid dynamics in building design: aspects and trends. Indoor and Built Environment, 15(4): p. 305-313.
2. Jiang, Y. and Q. Chen, 2002. Effect of fluctuating wind direction on cross natural ventilation in buildings from large eddy simulation. Building and Environment, 37(4): p. 379-386.
3. Farea, T., D. Ossen, and A. Isah, 2012. Common configuration of light-well in high-rise residential buildings in Kuala Lumpur, in 4th International Network for Tropical Architecture (iNTA). NUS: Singapore
4. Kotani, H., et al., 2003b. Environmental assessment of light well in high-rise apartment building. Building and Environment, 38(2): p. 283-289.
5. Prajongsan, P. and S. Sharples, 2012. Enhancing natural ventilation, thermal comfort and energy savings in high-rise residential buildings in Bangkok through the use of ventilation shafts. Building and Environment, 50(0): p. 104-113.
6. Givoni, B., 1998. Climate Considerations in Building and Urban Design. New York: Van Nostrand Reinhold.
7. Yuen, B. and A.G.O. Yeh, 2011. High-Rise Living in Asian Cities. London Springer.
8. Rajapaksha, I., H. Nagai, and M. Okumiya, 2003. A ventilated courtyard as a passive cooling strategy in the warm humid tropics. Renewable Energy, (28): p. 1755–1778.
9. Santamouris, M., 2006. Building ventilation : the state of the art. London: Earthscan.
10. Khan, N., Y. Su, and S.B. Riffat, 2008. A review on wind driven ventilation techniques. Energy and Buildings, 40(8): p. 1586-1604.
11. Aldawoud, A. and R. Clark, 2008. Comparative analysis of energy performance between courtyard and atrium in buildings. Energy and Buildings, 40(3): p. 209-214.
12. Ji, Y., M.J. Cook, and V. Hanby, 2007. CFD modelling of natural displacement ventilation in an enclosure connected to an atrium. Building and Environment, 42(3): p. 1158-1172.
13. Tominaga, Y., et al., 2008. AIJ guidelines for practical applications of CFD to pedestrian wind environment around buildings. Journal of Wind Engineering and Industrial Aerodynamics, 96(10-11): p. 1749-1761.
14. Allocca, C., Q. Chen, and L.R. Glicksman, 2003. Design analysis of single-sided natural ventilation. Energy and Buildings, 35(8): p. 785-795.
15. Haw, L.C., et al., 2012. Empirical study of a wind-induced natural ventilation tower under hot and humid climatic conditions. Energy and Buildings, 52(0): p. 28-38.
16. Liu, P.-C., B. Ford, and D. Etheridge, 2012. A modeling study of segmentation of naturally ventilated tall office buildings in a hot and humid climate. International Journal of Ventilation, 11(1): p. 29-42.
17. Etheridge, D., 2012. Natural Ventilation of Buildings Theory, Measurement and Design. Chichester: John Wiley & Sons, Ltd.
18. Tantasavasdi, C., Srebric, J., & Chen, Q., 2001. Natural ventilation design for houses in Thailand. Energy and Buildings, (33): p. 815-824.
19. Coffey, C.J. and G.R. Hunt, 2007. Ventilation effectiveness measures based on heat removal: Part 2. Application to natural ventilation flows. Building and Environment, 42(6): p. 2249-2262.
20. Fitzgerald, S.D. and A.W. Woods, 2008. The influence of stacks on flow patterns and stratification associated with natural ventilation. Building and Environment, 43(10): p. 1719-1733.
21. Kang, J.-H. and S.-J. Lee, 2008. Improvement of natural ventilation in a large factory building using a louver ventilator. Building and Environment, 43(12): p. 2132-2141.
22. Stathopoulou, O.I., et al., 2008. An experimental study of air quality inside large athletic halls. Building and Environment, 43(5): p. 834-848.
23. Xu, L. and T. Ojima, 2007. Field experiments on natural energy utilization in a residential house with a double skin façade system. Building and Environment, 42(5): p. 2014-2023.
24. Kuznik, F., G. Rusaouën, and J. Brau, 2007. Experimental and numerical study of a full scale ventilated enclosure: Comparison of four two equations closure turbulence models. Building and Environment, 42(3): p. 1043-1053.
25. Juárez, J.O., et al., 2011. Numerical study of natural convection in an open cavity considering temperature-dependent fluid properties. International Journal of Thermal Sciences, 50(11): p. 2184-2197.
26. Gan, G., 2010b. Interaction between wind and buoyancy effects in natural ventilation of buildings. The Open Construction and Building Technology Journal, (3): p. 134-145.
27. Gan, G., 2010a. Impact of computational domain on the prediction of buoyancy-driven ventilation cooling. Building and Environment, 45(5): p. 1173-1183.
28. Nugroho, A.M., 2009. Solar Chimney Geometry for Stack Ventilation in a Warm Humid Climate. International Journal of Ventilation, 8(2): p. 161-174.

29. Chen, Q., 2009. Ventilation performance prediction for buildings: A method overview and recent applications. Building and Environment, 44(4): p. 848-858.
30. Zhai, Z., et al., 2007. Evaluation of various turbulence models in predicting airflow and turbulence in enclosed environments by CFD: part 1: summary of prevalent turbulence models. HVAC & R Research, 13(6): p. 853–70.
31. Villi, G., W. Pasut, and M. Carli, 2009. CFD modelling and thermal performance analysis of a wooden ventilated roof structure. Building Simulation, 2(3): p. 215-228.
32. Ramponi, R. and B. Blocken, 2012a. CFD simulation of cross-ventilation for a generic isolated building: Impact of computational parameters. Building and Environment, 53(0): p. 34-48.
33. van Hooff, T. and B. Blocken, 2010. Coupled urban wind flow and indoor natural ventilation modelling on a high-resolution grid: A case study for the Amsterdam ArenA stadium. Environmental Modelling & Software, 25(1): p. 51-65.
34. Ramponi, R. and B. Blocken, 2012b. CFD simulation of cross-ventilation flow for different isolated building configurations: Validation with wind tunnel measurements and analysis of physical and numerical diffusion effects. Journal of Wind Engineering and Industrial Aerodynamics, 104–106: p. 408-418.
35. Jiang, Y., et al., 2003. Natural ventilation in buildings: measurement in a wind tunnel and numerical simulation with large-eddy simulation. Journal of Wind Engineering and Industrial Aerodynamics, 91(3): p. 331-353.
36. Jiang, Y. and Q. Chen, 2003. Buoyancy-driven single-sided natural ventilation in buildings with large openings. International Journal of Heat and Mass Transfer, 46(6): p. 973-988.
37. van Hooff, T., et al., 2011. A venturi-shaped roof for wind-induced natural ventilation of buildings: Wind tunnel and CFD evaluation of different design configurations. Building and Environment, 46(9): p. 1797-1807.
38. Liu, P.-C., H.-T. Lin, and J.-H. Chou, 2009. Evaluation of buoyancy-driven ventilation in atrium buildings using computational fluid dynamics and reduced-scale air model. Building and Environment, 44(9): p. 1970-1979.
39. Rundle, C.A., et al., 2011. Validation of computational fluid dynamics simulations for atria geometries. Building and Environment, 46(7): p. 1343-1353.
40. Baharvand, M., M. Hamdan Ahmad, and R. Abdul Majid, 2013. DesignBuilder Verification and Validation for Indoor Natural Ventilation. Journal of Basic and Applied Scientific Research (JBASR), 3(4): p. 8.
41. Ravikumar, P. and D. Prakash, 2011. Analysis of thermal comfort in a residential room with insect proof screen: A case study by numerical simulation methods. Building Simulation, 4(3): p. 217-225.
42. Ampofo, F. and T.G. Karayiannis, 2003. Experimental benchmark data for turbulent natural convection in an air filled square cavity. International Journal of Heat and Mass Transfer, 46(19): p. 3551-3572.
43. Mak, C.M., et al., 2007. A numerical simulation of wing walls using computational fluid dynamics. Energy and Buildings, 39(9): p. 995-1002.
44. Gan, G. and S.B. Riffat, 1998. A numerical study of solar chimney for natural ventilation of buildings with heat recovery. Applied Thermal Engineering, 18(12): p. 1171-1187.
45. Lesieur, Yaglom, and Davidson, 2001. New trends in turbulence Vol. 74. New York: Spriger.
46. Hussain, S., P.H. Oosthuizen, and A. Kalendar, 2012. Evaluation of various turbulence models for the prediction of the airflow and temperature distributions in atria. Energy and Buildings, 48: p. 18-28.
47. Kotani, H., R. Satoh, and T. Yamanaka, 2003. Natural ventilation of light well in high-rise apartment building. Energy and Buildings, 35(4): p. 427-434.
48. Franke, et al., 2007. Best practice guideline for the CFD simulation of flows in the urban environment, in COST. Meteorological Institute, University of Hamburg, Germany.
49. Asfour, O.S., 2010. Prediction of wind environment in different grouping patterns of housing blocks. Energy and Buildings, 42(11): p. 2061-2069.
50. Ferziger, J.H. and M. Peric, 2002. Computational Methods for Fluid Dynamics. New York Springer.
51. Wilcox, D.C., 1998. Turbulence modeling for CFD. Vol. 2. California: DCW industries
52. Zikanov, O., 2010. Essential computational fluid dynamics. Hoboken, NJ: Wiley.
53. Versteeg, H.K. and W. Malalasekera, 2007. An Introduction To Computational Fluid Dynamics: The Finite Volume Method. Harlow: : Pearson Education.
54. ANSYS®, 2011. Fluent theory guide, in 14.0. ANSYS, Inc: USA.

Appendix: Model equation parameters for the various turbulence models

Model	ϕ	Γ_ϕ	S_ϕ	Coefficients
Continuity	1	0		
Momentum	u_i	$\mu+\mu_t$	$-\frac{\partial\rho}{\partial x_i}-\rho g$	Notes: $S_{ij}=\frac{1}{2}\left(\frac{\partial u_j}{\partial x_i}+\frac{\partial u_i}{\partial x_j}\right)$, $\Omega_{ij}=\frac{1}{2}\left(\frac{\partial u_i}{\partial x_j}+\frac{\partial u_j}{\partial x_i}\right)$
Energy	T	$\frac{\mu}{Pr}+\frac{\mu_t}{Pr_t}$	S_T	
SA	$\tilde{\nu}$	$\mu+\rho\tilde{\nu}$	$G_\nu+\tilde{\nu}^*-Y_\nu$	$\mu_t=\rho\tilde{\nu}f_{v1}$, $G_\nu=C_{bi}\rho\tilde{S}\tilde{\nu}$, $\tilde{\nu}^*=\frac{C_{b2}}{\sigma_{\tilde{\nu}}}\rho\left(\frac{\partial\tilde{\nu}}{\partial x_j}\right)^2$, $Y_\nu=C_{w1}\rho f_w\left(\frac{\tilde{\nu}}{d}\right)^2$,
STD *k-ε*	k	$\mu+\frac{\mu_t}{\sigma_k}$	$G_k+G_b-\rho\varepsilon$	$\mu_t=\rho C_\mu\frac{k^2}{\varepsilon}$, $G_k=\mu_t S^2$, $S=\sqrt{2sS_{ij}S_{ij}}$ $G_b=-9\frac{\mu_t}{\rho\,\mathrm{Pr}_t}\frac{\partial p}{\partial x_i}$. $C_\mu=0.09$, $C_{1\varepsilon}=1.44$,
			$C_{1\varepsilon}\frac{\varepsilon}{k}(G_k+C_{3\varepsilon}G_b)$	
	ε	$\mu+\frac{\mu_t}{\sigma_\varepsilon}$	$-C_{2\varepsilon}\rho\frac{\varepsilon^2}{k}$	$C_{2\varepsilon}=1.92$, $\Gamma_k=1.0$, $\Gamma_\varepsilon=1.3$
RNG *k-ε*	k	$\alpha_k\mu_{eff}$	$C_{1\varepsilon}\frac{\varepsilon}{k}(G_k+C_{3\varepsilon}G_b)$	$\alpha_k=\alpha_\varepsilon=1.393$, $\mu_{eff}=\mu_t=\rho C_\mu\frac{k^2}{\varepsilon}$, $R_3=\frac{C_\mu\rho\eta^3(1-\eta/\eta_0)}{1+\beta\eta^3}\frac{\varepsilon^2}{k}$, $C_\mu=0.0845$, $\eta=\frac{S_k}{\varepsilon}$,
	ε	$\alpha_\varepsilon\mu_{eff}$	$-C_{2\varepsilon}\rho\frac{\varepsilon^2}{k}-R_3$	$\eta_0=4.38$, $\beta=0.012$
SST *k-ω*	k	$\mu+\frac{\mu_t}{\sigma_k}$	$\tilde{G}_k-Y_k$	$\mu_t=\frac{\rho k}{\omega}\frac{1}{\max\left(1/\alpha^*, SF_2/a_1\omega\right)}$, $\tilde{G}_k=\min(G_k,10\rho\beta^*k\omega)$, $Y_k=\rho\beta^*k\omega$, $G_\omega=\frac{\alpha_\infty}{\gamma_t}\tilde{G}_k$,
	ω	$\mu+\frac{\mu_t}{\sigma_\omega}$	$G_\omega-Y_\omega+D_\omega$	$Y_\omega=\rho\beta\omega^2$, $D_\omega=2(1-F_1)\rho\frac{1}{\omega\sigma_{\omega,2}}\frac{\partial k}{\partial x_j}\frac{\partial\omega}{\partial x_j}$,
SST	γ	$\mu+\mu_t/\sigma_\gamma$	$P_{\gamma1}-E_{\gamma1}+P_{\gamma2}-E_{\gamma2}$	$\mu_t=\frac{\rho k}{\omega}$, $P_{\gamma1}=C_{a1}F_{length}\,\rho S\left[\gamma F_{onset}\right]^{c\gamma3}$, $E_{\gamma1}=C_{e1}P_{\gamma1}\gamma$, $E_{\gamma2}=C_{e2}P_{\gamma2}\gamma$, $\sigma_\gamma=1.0$;
	$R\tilde{e}_{\theta t}$	$\sigma_\theta(\mu+\mu_t)$	$P_{\theta t}$	$P_{\theta t}=c_{\theta t}\rho/t(Re_{\theta t}-R\tilde{e}_{\theta t})(1.0-F_{\theta t})$, $G_k^*=\gamma_{eff}\tilde{G}_k$, $Y_k^*=\min\left(\max\left(\gamma_{eff},0.1\right),1.0\right)Y_k$, $\sigma_{\theta t}=2.0$;
	k	$\mu+\mu_t/\sigma_k$	$G_k^*-Y_k^*$	
RSM	$\overline{u_i'u_j'}$	$\mu+\frac{\mu_t}{\sigma_k}$	$P_{ij}+G_{ij}+\phi_{ij}-\varepsilon_{ij}$	$P_{ij}=-\rho\left(\overline{u'_iu'_k}\frac{\partial u_j}{\partial x_k}+\overline{u'_ju'_k}\frac{\partial u_i}{\partial x_k}\right)$, $G_{ij}=-\rho\beta(g_i\overline{u'_jT}+g_j\overline{u'_iT})$, $\phi_{ij}=\overline{p'\left(\frac{\partial u'_i}{\partial x_j}+\frac{\partial u'_j}{\partial x_i}\right)}$, $\varepsilon_{ij}=\frac{2}{3}\varepsilon\delta_{ij}$

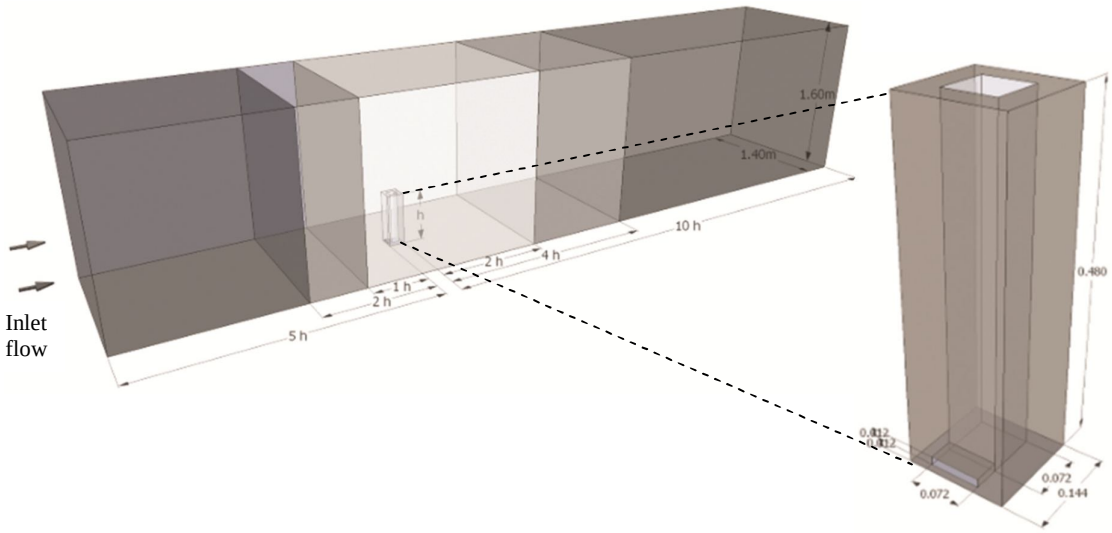

Fig.1 Perspective view of the different sizes of computational domain used in the numerical study and the building model used by Kotani et al. [47].

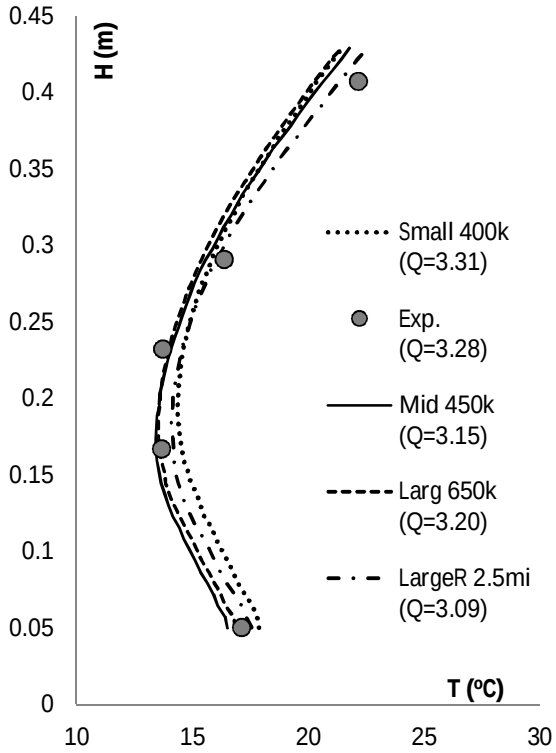

Fig.2 Temperature distribution (T) and airflow rate (Q) along the height (H) of the lightwell in four different simulation domain sizes; small, medium (Mid), large and largest as recommended (LargeR) , compared with experimental data (Exp.) for different number of meshes ranging from $40x10^4$(400k) to $2.5\ x10^6$ (2.5mi)

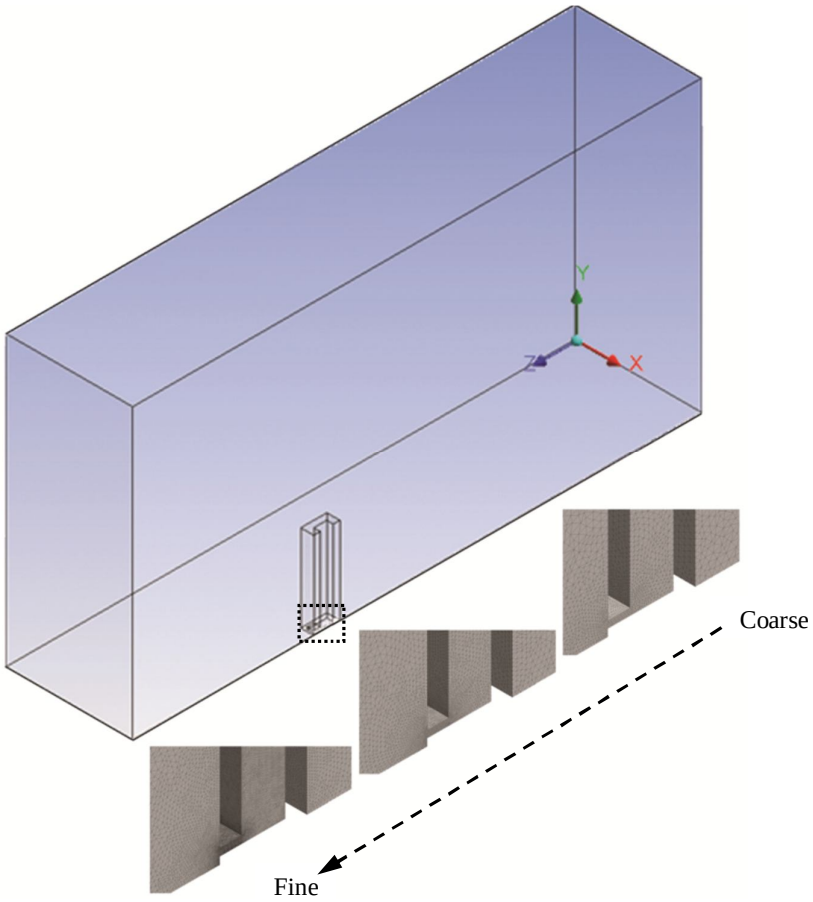

Fig. 3 Mesh grid-independence test using symmetry configuration of the building model and domain with enlarged views of the different mesh structures at the bottom zone of the lightwell

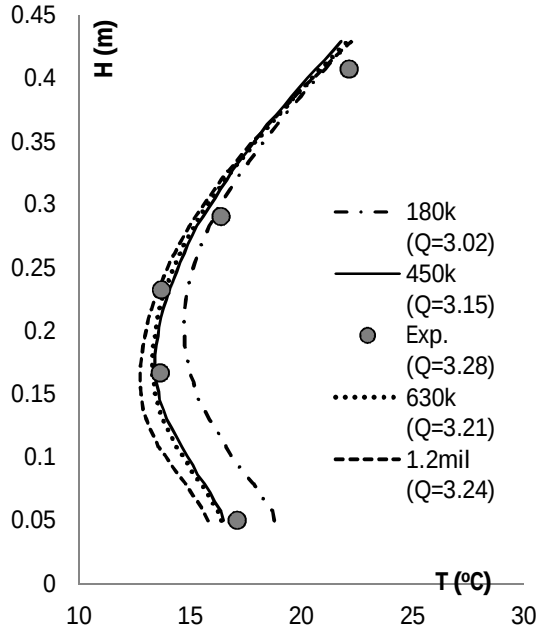

Fig.4 Air temperature distribution (T) and airflow rate (Q) along the height (H) of the lightwell for four types of meshes, ranging from coarse $18x10^4$ (180k) to fine 1.2×10^6(1.2 mil) compared with experimental data (Exp.) using RNG k-ε model

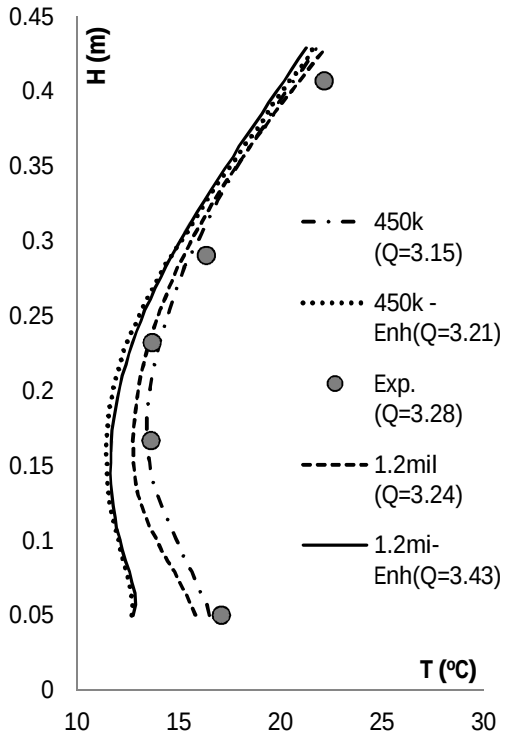

Fig.5 Temperature distribution (T) and airflow rate (Q) along the height (H) of the lightwell for near-wall treatment adopting the standard wall function and the enhanced wall (Enh) treatment for different mesh sizes (coarse (450k) and fine (1.2 million)), using the RNG *k-ε* model

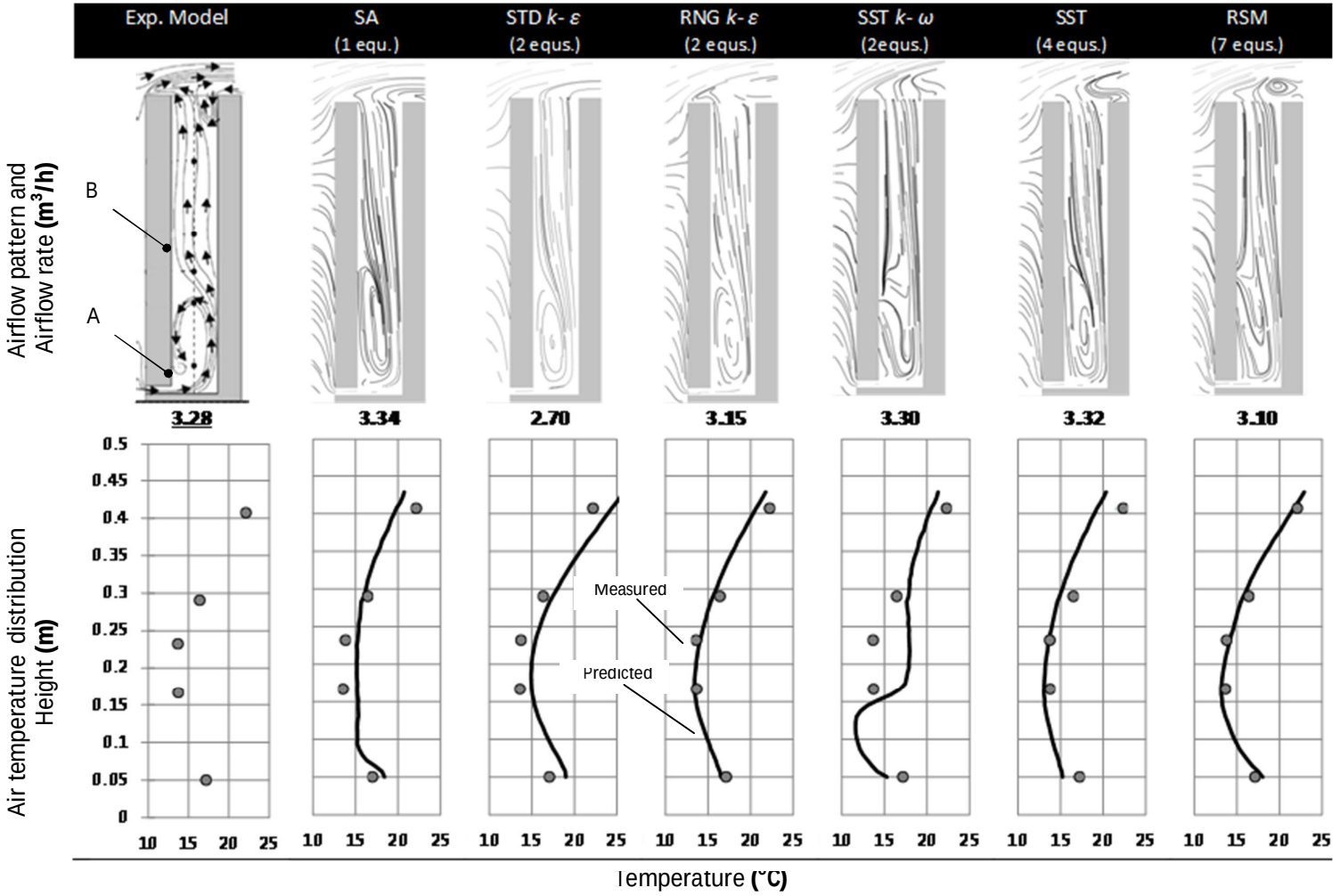

Fig. 6 Numerical results of airflow pattern, airflow rate and air temperature distribution in the lightwell for various turbulence models compared with experimental data.